New Journal of Physics
The open access journal at the forefront of physics

Deutsche Physikalische Gesellschaft DPG IOP Institute of Physics

PAPER • OPEN ACCESS

Sputtering and redeposition of ion irradiated Au nanoparticle arrays: direct comparison of simulations to experiments

To cite this article: Henry Holland-Moritz *et al* 2017 *New J. Phys.* **19** 013023

View the article online for updates and enhancements.

Related content

- Introduction to Focused Ion Beam Nanometrology: Ion–solid interactions
D C Cox
- Enhanced sputter yields of ion irradiated Au nano particles: energy and size dependence
Henry Holland-Moritz, Sebastian Scheeler, Christoph Stanglmair et al.
- Ion beam irradiation of nanostructures: sputtering, dopant incorporation, and dynamic annealing
Andreas Johannes, Henry Holland-Moritz and Carsten Ronning

This content was downloaded from IP address 210.13.70.28 on 13/10/2017 at 14:47

New Journal of Physics
The open access journal at the forefront of physics

Deutsche Physikalische Gesellschaft DPG
IOP Institute of Physics

Published in partnership with: Deutsche Physikalische Gesellschaft and the Institute of Physics

CrossMark

OPEN ACCESS

RECEIVED
12 June 2016

REVISED
9 December 2016

ACCEPTED FOR PUBLICATION
5 January 2017

PUBLISHED
20 January 2017

Original content from this work may be used under the terms of the Creative Commons Attribution 3.0 licence.

Any further distribution of this work must maintain attribution to the author(s) and the title of the work, journal citation and DOI.

PAPER

Sputtering and redeposition of ion irradiated Au nanoparticle arrays: direct comparison of simulations to experiments

Henry Holland-Moritz[1,3], **Andrey Ilinov**[2], **Flyura Djurabekova**[2], **Kai Nordlund**[2] **and Carsten Ronning**[1]

[1] Institute of Solid State Physics, University of Jena, Max-Wien-Platz 1, D-07743 Jena, Germany
[2] Department of Physics, University of Helsinki, PO Box 43, FI-00014, Finland
[3] Author to whom any correspondence should be addressed.

E-mail: henry.holland-moritz@uni-jena.de

Keywords: sputtering, redeposition, ion beam modification, nanoparticles

Supplementary material for this article is available online

Abstract

Ion beam processing of surfaces is well known to lead to sputtering, which conventionally is associated only with erosion of atoms from the material. We show here, by combination of experiments and a newly developed Monte Carlo algorithm, that in the case of nanoparticles in a regular two-dimensional array on surfaces, the redeposition of sputtered atoms may play a significant role on the system development. The simulations are directly compared to *in situ* experiments obtained using a dual focused Ga^+ ion beam system and high resolution scanning electron microscopy, and explain the size evolution by a combination of sputtering and redeposition of sputtered material on neighboring particles. The effect is found to be dependent on the size of the nanoparticles: if the nanoparticle size is comparable to the ion range, the reposition is negligible. For larger nanoparticles the redeposition becomes significant and is able to compensate up to 20% of the sputtered material, effectively reducing the process of sputtering. The redeposition may even lead to significant growth: this was seen for the nanoparticles with the sizes much smaller than the ion range. Furthermore, the algorithm shows that significant redeposition is possible when the large size neighboring nanoparticles are present.

1. Introduction

In the past years, nanostructures have attracted intense research interest due to their new properties not seen in bulk counterparts [1–3]. Ion irradiation is a powerful tool to tune the properties of materials [4–7] for a wide range of applications [8–12]. In many cases, ion implantation is also the method of choice for doping nanostructures, since this method is not constrained by thermal equilibrium [4, 13, 14]. Ion-solid interaction in bulk structures is theoretically well understood [15–17], however nanostructures offer new challenges. For instance, the large surface-to-volume ratio of nanostructures leads to enhanced sputter yields compared to bulk structures [18–20], which can change e.g. the expected doping concentration [4]. Although experiments are the most reliable source of knowledge, simulation methods are often useful to obtain insight on mechanisms behind the ion-solid interaction. A variety of Monte Carlo (MC) codes are available for bulk and layered geometries [15, 21, 22]; among these, new codes were recently proposed to take the 3D geometry of the target into account, which is necessary to describe ion–solid interactions in nanostructures [23, 24].

Recently, ion irradiation of individual nanoparticles (NP) and nanorods has attracted research interest [20, 25, 26]. However, in typical experimental conditions and for practical applications, the NPs are built in an array rather than a single isolated nanostructure [28]. In such cases, one has to take into account the probability of redeposition of sputtered material on neighboring NPs. This quantity depends on the interparticle distance, the patterning order and particle size. Redeposition was previously investigated in context of surface structuring using ion beams, which are essentially 2D systems, where it has a significant influence on the formation of regular surface patterns [27, 28]. The effect of redeposition also plays a key role in ion etching of microstructures

© 2017 IOP Publishing Ltd and Deutsche Physikalische Gesellschaft

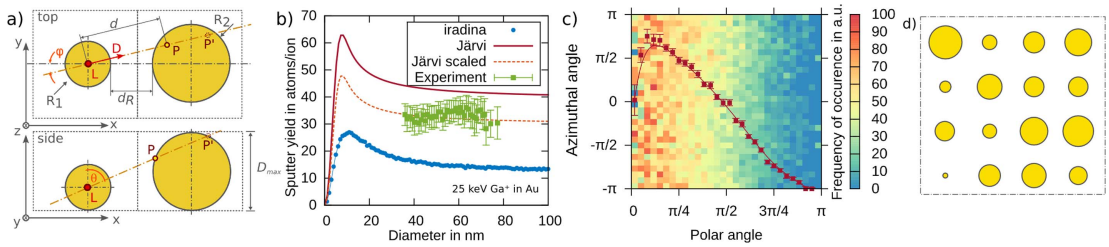

Figure 1. (a) Schematic illustration of the geometry in top view for the simulation of two NPs. L marks the leaving point inside NP 1, $\boldsymbol{D}$ is the direction vector of the leaving atom, P and P' are the intersection points of the line defined by $\boldsymbol{D}$. The distance d is the distance between the nearest intersection points of the line on NP 1 and 2 (note, here only the projection is shown), d_R is the rim-to-rim distance of the NPs. (b) Sputter yields versus NP diameter. The blue curve shows the sputter yield calculated by iradina, the red curve shows the results of the model by Järvi *et al* [18]. The data points plotted in green are the results from the experiment presented in [31]. The dashed orange curve is the sputter yield by Järvi scaled to fit the experimental sputter yield. (c) Angular distribution map of sputtered atoms for the irradiation of a Au NP with 50 nm diameter with 25 keV Ga^+ ions. The colors of the map code the amount of atoms in a certain direction. Additionally, the average number of atoms over the azimuthal angle in a certain polar direction is plotted in red. (d) Schematic example image of the simulated 4 × 4 square pattern with randomly distributed NP sizes.

[29] and focused ion beam (FIB) milling, where the redeposition influences the formation of high-aspect ratio nanostructures [30]. The processes discussed in the literature appear at high fluence irradiations of surfaces.

In this article, we report on a detailed study of redeposition of atoms sputtered from a population of 3D gold (Au) NPs organized on a substrate as a patterned lattice by *in situ* experiments using high resolution scanning electron microscopy (SEM) at low fluence irradiation. Additionally, a MC simulation code was developed for this specific purpose to get a deeper insight into the redeposition process. The results of experiments and simulation are directly compared to each other.

2. Methods

2.1. Development of a MC simulation code

A MC code was developed to enable a detailed study of the redeposition of sputtered material on neighboring NPs. For this purpose, the simulations were designed to emulate the irradiation process of several Au NPs placed in a regular pattern on a flat substrate. Gallium (Ga^+) was chosen as an ion species, since it is the most common ion species in FIB systems and was used for the *in situ* experiments presented in this work. The algorithm is summarized in the appendix.

The simulation box had square geometry with the lateral size $l_x \times l_y$ and contained NPs of different sizes arranged in a square patterned lattice. Here, the volume of the entire simulation box was divided into equally sized squared cells to host each NP. The height of all cells was the same and was defined by the diameter of the largest particle. In most cases, the NP sizes were randomly chosen according to the distribution obtained from experimental data [31]. In the z direction, the particles were positioned at the bottom of the simulation volume, as shown in figure 1(a), side view. In the x–y plane, the particles were centered in their respective cells. The cell size, therefore, determines the inter-particle distance.

The redeposition of an atom sputtered from the NP marked as NP 1 on the NP marked NP 2 is schematically drawn in figure 1(a) and modeled as follows. At first one NP is selected to receive an ion impact. The position of the impact (x_i, y_i) was randomly selected within the simulation area. If the NP is hit, the sputtering yield is given by figure 1(b) as a function of a diameter for spherical Au NPs irradiated with Ga^+ ions with an ion energy of 25 keV. Here, two different routes were used to describe the sputtering yield of Au NPs. In figure 1(b), the blue dots show the sputtering yields calculated by the three-dimensional BCA code *iradina* [23] and the red ones are the results of the semi-analytical model by Järvi *et al,* which is based on Sigmund's general surface model [32], integrated for the 3D surface of a spherical NP (hereafter referred to as Järvi's model). Järvi's model was originally parameterized by molecular dynamics simulations [18, 33]. As one can see, the sputtering yields given by Järvi's model are up to four times higher than the sputtering yields calculated by *iradina*. The differences between the model by Järvi *et al* and *iradina* originate from the fact that *iradina* is a BCA code which neglects many-body atomic interactions. Since the model by Järvi *et al* is based on MD simulations, it is capable of modeling sputtering processes more realistically. Järvi *et al* used the universal ZBL potential for low distance interatomic interactions [18]. However, since the sputtering in the MD is dominated by thermal effects, the choice of the repulsive potential is not expected to affect the results significantly. Since MD simulations take thermally driven effects into account, which is reported to be the main contribution to the sputter yield [26] and neglected in *iradina*, the model by Järvi *et al* shows a larger sputter yield compared to the BCA simulation results.

Experimental data for this situation are available in [31], and the data is shown in figure 1(b) as green dots in between the two calculations. Järvi's model was then scaled by a factor of 0.77 to agree with the experimental data. This coefficient was determined by minimizing the root mean square error between the values given by the scaled Järvi's model and the experimental yield values, for NPs having diameters above 35 nm. The experimental sputter yields appear to be smaller compared to Järvi's model due to the fact that the model takes a single, freestanding NP into account, while the experimental situation is more complex due to particle–particle and particle–substrate interactions, which lower the sputter yield. It is also possible that this ~20% difference arises from shortcomings in the interatomic potential, since the Järvi model was fit to the bulk yield which in other studies has been found to somewhat depend on the interatomic potential [34]. The maxima of all curves are at sizes around 10 nm, which coincides well with the ion range of the used ions.

Thus, the number of sputtered atoms is taken from these distributions given by the sputtering model in use, and defined by the size of the NP that was 'hit' by the incoming ion. In the following, each sputtered atom is considered up to the total sputtering yield.

The origin of the sputtered atoms is in the center of the NP. The direction (Θ, ϕ) to where a sputtered atom will fly, where Θ is the polar and ϕ the azimuthal angle, was calculated by the size dependent angular distribution of sputtered atoms. This distribution was obtained by simulations performed with *iradina* for various NP sizes ranging from 1 to 100 nm for random ion impacts on spherical, free standing NPs. One sample distribution for a NP with a diameter of 50 nm is shown in figure 1(c) as a function of Θ and ϕ. One can see that the distribution is symmetric in the azimuthal direction, which can be expected for random impacts into spherical NPs. Additionally, the average value of the number of sputtered atoms in a certain polar direction is shown by the red curve in figure 1(c). The angular distribution shows a preferential emission towards polar angles smaller than $\pi/2$. The maximum is shifted towards polar angles larger than 0, which indicates the maximum for the irradiation of flat surfaces, due to the curvature of the NPs and lateral sputtering [20]. In the simulation, the azimuthal angle is uniformly randomized between 0 and 2π, while the distribution of the polar angles depends on the particles size with the shift towards the opposite direction of the beam with increasing particle size (not shown here). The reason for this is that ions of a certain energy have a certain penetration depth in the material. If the size of the particle increases and surpasses the average ion range in the material, the situation is becoming similar to sputtering of bulk targets. Sputtering then occurs more likely in the backward direction, which is in line with the bulk situation. For computational efficiency, the angular distribution and sputter yield are randomly selected from a distribution for random ion impacts, although the sputter yield as well as the angular distribution of the sputtered atoms for every ion impact depend on the impact position on the NP [20]. However, since the number of ion impacts on a NP during irradiation is of the order of 10^4, it is reasonable to assume that the differences due to the impact positions will not affect the behavior of the growth dynamics of NPs to improve of the simulations.

After the direction is found, the next step is to define the probability of redeposition of neighboring NPs. The sputtered atom is considered as 'redeposited', if the direction vector of this atom intersects a NP in the simulation volume, as shown in figure 1(a). The diameter of the NP, where the redeposited atom lands, is then recalculated by adding one atomic volume V_a to the volume; $V_P = V_P + V_a$, and then recalculating the diameter for the new volume. Similarly, the diameter of the sputtered particle at R_1 is reduced corresponding to a volume reduction by $Y \cdot V_a$ for each sputtering event.

The travel distance of a sputtered atom was done up to a cut-off distance, if the atom is traversing the simulation volume almost parallel to the *x–y* plane without hitting a particle. Test simulations showed that a cut-off distance of 500 nm is suitable. This value was fixed for all simulations showed here. If the sputtered atom is intersecting the plane at $z = 0$ or $z = D_{max}$, the atom is not followed anymore. If the line of direction intersects the simulation volume side plane, periodic boundary conditions (PBC) were applied. The starting point of the direction vector is set to the new entry point in the simulation volume and the loop over the NPs starts again.

The number of simulated ion impacts was calculated by the ion fluence times the area in the *x–y* plane of the simulated cells. The main simulation loop runs over the number of ions. The redeposition was simulated for a two-dimensional NP array on a squared 4×4 grid with a side length of 95 nm. This is the average distance of the centers of the Au NPs in the samples investigated experimentally in [31]. The particles were located at the center of these squares. The simulation for 16 NPs was performed 120 times with different random seeds to achieve reasonable statistics. The NP sizes were randomly chosen from the size distribution obtained from the samples investigated in experiments [31], shown in figure 2(a) in red. The NP sizes ranged from 20 to 80 nm and were distributed with a Gaussian distribution with a mean value of 51 nm and a standard deviation of 7.6 nm. An example image of a randomly generated pattern is shown in figure 1(d). It is not very likely that small particles with sizes smaller than 20 nm appear in the simulation using the given size distribution. As an additional test case to achieve a better understanding of size dependence of the results, we also investigated a set of smaller NP with the sizes below 20 nm with a reasonable number of NPs, the mean value of the Gaussian distribution was set to 25 nm with a standard deviation of 20 nm. All simulations were performed using Järvi's and scaled Järvi's model

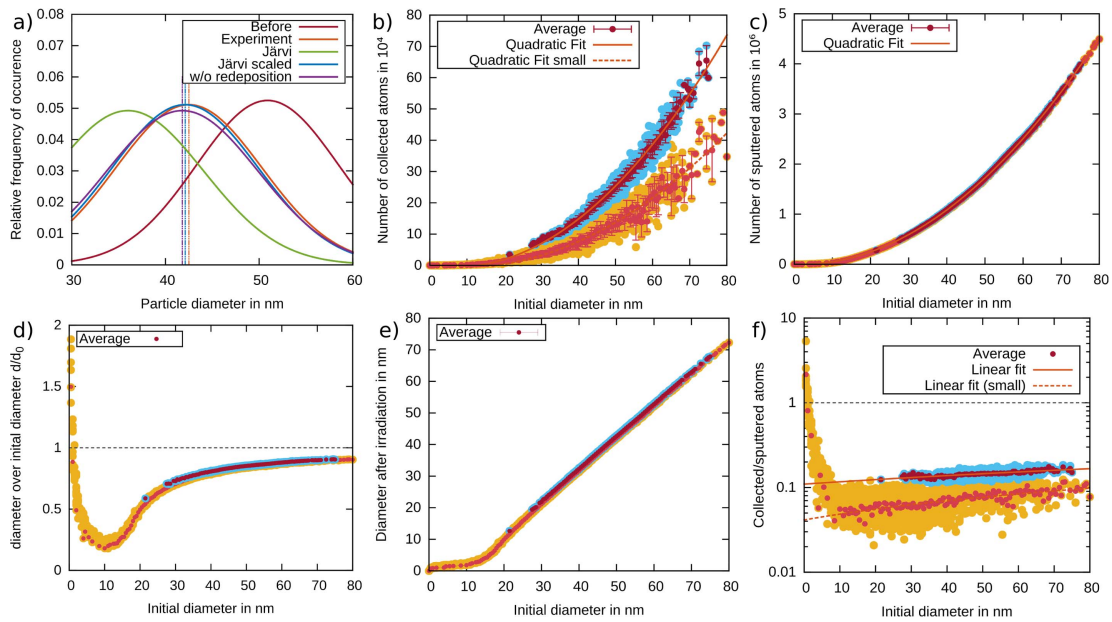

Figure 2. (a) Gaussian fits of the size distributions of the particles before (red, experiment) and after irradiation (both experiment and simulation). The irradiated cases are all to the same fluence of 3×10^{15} ions cm^{-2}. The orange distribution shows the experimental distribution after the irradiation. The green curve shows the simulation result using the Järvi's model, while the results shown in blue show the results using the scaled Järvi's model. The purple curve shows the simulation results without redeposition using the scaled Järvi model. The dashed vertical lines represent the mean values of the respective distributions. (b) Number of gained atoms as a function of the particle size. The blue points show the results for single NPs with a size distribution with a mean diameter of 50 nm, while the yellow points show the results for single NPs with a size distribution of a mean diameter of 25 nm. The red points show the mean value for certain NP sizes. The orange curves show fits of quadratic functions of the average data points. The error bars show the standard error of the mean. (c) Total number of sputtered atoms as a function of the NP size. The orange curve shows the quadratic fit of the mean values of the data points. (d) Ratio of the NP diameter after and before the simulated sputtering as a function of the particle size. (e) NP diameter as a function of the initial particle size. (f) Ratio of gained versus sputtered atoms as a function of the initial particle size. The color coding in figures (c)–(f) is the same as in (b).

for the total sputtering yields. To understand the role of redeposition, we also carried out a set of test simulations with the redeposition turned off.

2.2. Experiments

The gold NP arrays on a Si substrate with a native oxide layer were fabricated by wet-chemical synthesis of Au NPs using seed growth and spin-coating [35]. The irradiation experiments presented in this work were adapted from [31] and performed in a FIB system using 30 keV Ga^+ ions. The total irradiated ion fluence was 5×10^{15} cm^{-2}. The total irradiated area was 3×3 μm^2. The ion beam was defocused to prevent the immediate destruction of the NPs. SEM images were taken every 8×10^{13} cm^{-2} over the process of irradiation, which corresponds to approximately 60 SEM images in total. The ion current was set to 1 pA to avoid thermally driven effects observed in previous experiments and described in [14, 31]. The geometrical data of the SEM images were extracted by *imagej* [36]. The NP diameter was estimated by measuring the cross section area A of the particles. The particles were assumed to be spherical and the diameter was calculated by $d = \sqrt{4A/\pi}$. As coordinates of the particles on the arrays, the centers of mass of the SEM image were used. In the y direction, the coordinates from the SEM images were corrected by the viewing angle of 52° in the SEM. The sputtering yields were calculated as described in [14, 31]. The results of both experiment and simulation are still comparable for the used energies, since the difference in the sputtering yield for 25 and 30 keV Ga^+ irradiation is negligible [31].

3. Results and discussion

3.1. Statistic results

The size distribution of Au NPs after irradiation of both the simulations and experiment are shown in figure 2(a) (for clarity, only the Gaussian fits are shown). At first, one can observe that the Gaussian shape of the size distribution is conserved in all cases after irradiation. Second, the mean value of the diameters is shifted to smaller values compared to the initial distribution due to sputtering (compare table 1). Both scaled and unscaled Järvi's model slightly underestimates (by ~0.4 and 6.5 nm, respectively) the resulting size distribution of the NPs. If the sputtering process was simulated without redeposition using the scaled Järvi's model, the mean value

Table 1. Mean sizes and standard deviations of the ion irradiated particles before and after simulated and experimental irradiation with a fluence of 3×10^{15} ions cm^{-2}. The results without redeposition were obtained by using scaled Järvi's model.

	Before	Experiment	Järvi	Järvi scaled	w/o redeposition
d (nm)	50.9	42.5	36.0	42.1	41.8
σ (nm)	7.6	7.8	8.1	7.8	8.1

is 0.7 nm smaller than the mean value of the experimental results and matches almost the scaled Järvi results with redeposition. This leads to a difference of only 0.3 nm between the results with and without redeposition.

In the following only the results using the scaled Järvi's model are shown and discussed. The number of redeposited, thus gained, atoms as a function of the NP size is plotted in figure 2(b). The data are divided into two parts. The upper data points shown in blue represent the simulation results using the experimental arrays with NP size distribution with a mean diameter of 50 nm. The lower data points drawn in yellow show the simulation results for an array with a size distribution with a smaller mean diameter of 25 nm. The blue and yellow points represent the data points for single NPs, while the red and orange points indicate the mean values for the given diameter values. One can observe that both simulated regimes do not overlap. The reason is simply the smaller area coverage of the simulation volume by NPs using the size distribution with mean diameter of 25 nm. Therefore, the number of ions hitting the NPs and thus the total number of atoms sputtered and redeposited is reduced compared to size distributions with a mean diameter of 50 nm. The larger the covered area by NPs is, the more ions hit the NPs in total. This leads to a larger number of sputtered atoms, i.e. so the total number of gained atoms is increased.

However, the number of sputtered atoms shows the same quadratic relation for both simulations as a function of the NP size, as shown in figure 2(c). Indeed, one would expect a slight increase of the number of sputtered atoms for smaller NPs, since the sputtering yield shows a strong increase for NP sizes smaller than 20 nm. This effect is compensated by the lower ion impact probability, resulting in a small number of total sputtered atoms from NPs smaller than 20 nm and a conservation of the quadratic dependence of the number of sputtered atoms independent of the mean NP size.

The influence of the different sputtering yields as a function of diameter can be clearly seen in figure 2(d). Here, the ratio of the NP diameters before and after the irradiation is plotted versus the initial NP diameter, which shows a distinct minimum at ~10 nm. These NPs had the highest sputtering yield compared to all other sizes (figure 1(b)). From this plot one can see that the increased sputtering yield for small NP sizes has a strong influence on the relative change of the NP size. Since the sputtering yield shows an approximately constant behavior for NP sizes larger than 20 nm, the diameter after the irradiation shows an almost constant change of ~0.8 in this size range.

Figure 2(e) shows the absolute value of NP diameters after the irradiation plotted versus the initial ones. Here, a distinct kink is also observed around 10 nm. Thus, both figures 2(d) and (e) demonstrate that the general behavior changes at a NP size when the sputtering yield is maximal. Indeed a minimum appears in figure 2(d) at about the size where the sputter yield is maximal. Most interestingly, the values increase also for very small NPs and even turn to the growth of very small NPs with a size of ~1 nm. Several very small NPs with diameters smaller than 2 nm in the simulations showed a larger size after the irradiation compared to their initial size. In figure 2(f), the ratio of collected versus sputtered atoms is plotted over the NP size in a logarithmic scale. Beside the non-overlapping of the two size regimes, as already visible in figure 2(b), one can observe that there is a large variation of the ratio of collected versus sputtered particles for single NPs, which might be explained by the different sizes of the neighboring NPs. This is discussed in detail later in section 3.3. It is noticeable that the ratio increases linearly for increasing particle sizes for the whole simulated size range of the large mean NP diameter size distribution. In contrast to the large NPs, the data of the small NPs is only fitted for NP sizes larger than 10 nm, since the ratio of collected versus sputtered atoms shows a steep increase for NP sizes smaller than 10 nm. For the size distribution with large mean diameter, the value for fraction of redeposition varies from 12% to 18%, whereas the fraction for the simulation with small NPs are typically in the lower percent region. The slope of the linear fit is steeper for large NPs compared to small ones. The linear behavior is changing for NPs smaller than 10 nm for the same reasons as explained previously. Although in the experiments, NPs arrange in a regular manner on the surface, an assumption of a square lattice may appear rather crude. To analyze the effect of the chosen geometry, additional simulations with NPs arranged/positioned randomly on a plane had been performed, which led to qualitatively and quantitatively comparable results.

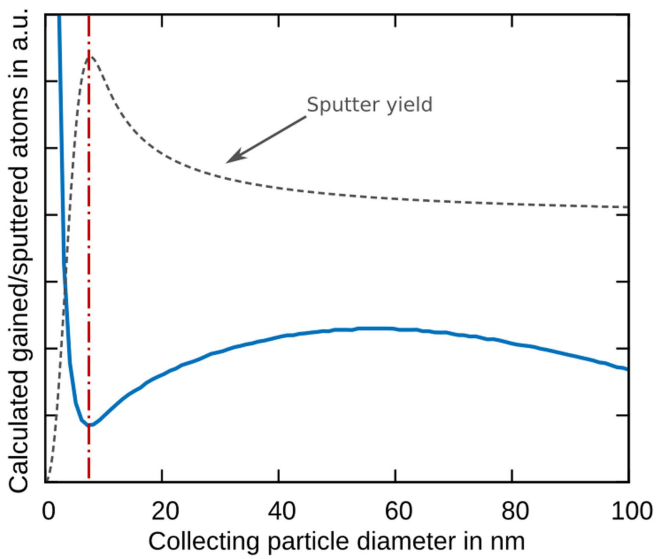

Figure 3. Calculated qualitative ratio of gained versus sputtered atoms as a function of the particle size. The dashed gray line shows the sputter yield in a.u., the dashed red line indicates the location of the maximum of the sputter yield.

3.2. Analytical estimate of the size dependence of redeposition

One has to consider the probabilities for atoms to sputter and to redeposit in order to understand the behavior depicted in figures 2(d) and (f). The probability to gain atoms due to redeposition can be estimated from the solid angle covering along the direction vector of the sputtered atom. The probability of sputtering, defined by the probability of a NP to be hit by an ion, is the ratio of the cross sectional area to the area of the simulation cell per particle. Thus, to model the ratio of gained atoms to sputtered ones, the probabilities of gaining atoms and ion impacts can be compared. The ion impacts have to be weighted with the sputtering yield. The result is shown in figure 3. The data f in this plot is analytically calculated as

$$f = \frac{\Omega(R_1, R_2, d^2)}{A(R_1) \cdot Y_n},$$

where Ω is the solid angle, A the cross sectional area of the NP, Y_n is the sputtering yield function, normalized to the maximum sputtering yield, d the distance between the NPs and R_1 and R_2 are the respective NP radii. The calculations shown here were obtained by using an interparticle distance of 95 nm, and an equal size of collecting and sputtering NP's of 50 nm. The trend of the curve is similar to the one of the average data points shown in figure 2(f) for small NPs.

The minimum of the calculated curve matches the maximum of the sputtering yield, similar to the simulation results. For the NP with diameters smaller and larger than 7.6 nm, the ratio of gained versus sputtered atoms is increasing, as already shown by the simulation. In the simulations, the ratio is increasing linearly with increasing particle diameter, while the calculated curve is increasing nonlinearly up to a maximum. The trend of the curve can be explained by the competition of both effects, sputtering and redeposition. On one hand, the probability of getting hit by an ion is decreasing with the decreasing NP size. On the other hand, the probability of collecting atoms by NPs is decreasing in the same way, since both events depend on the cross sectional area of the NP. Which effect is dominant is determined by the size distribution of NPs around the NP hit by an ion, as the simulations show for the different size distributions in figures 2(d) or (f).

In particular, figure 2(f) shows that the slope of the linear fit is decreasing with decreasing mean diameter of the size distribution. Since both the cross sectional area and the solid angle depend on the square of the diameter, one would indeed expect that the ratio of these parameters must have a linear behavior with increasing size. First, the size dependence of the sputtering yield changes the behavior of small NPs in benefit of the redeposition effect, since the sputtering yield is decreasing faster for NP sizes smaller than 7 nm. Secondly, the assumed dependence of the solid angle on particle size of the NP emitting atoms was not taken into account explicitly in this estimation. The isotropic emission of atoms due to the sputtering process is not the case in the simulation. In simulations, the redeposition effect may have fairly anisotropic nature, since in many cases the sputtered atoms are more likely to leave a NP in the direction of another NP in polar direction. These effects may explain the differences between the analytical estimation of the ratio of gained and sputtered atoms and the simulation results.

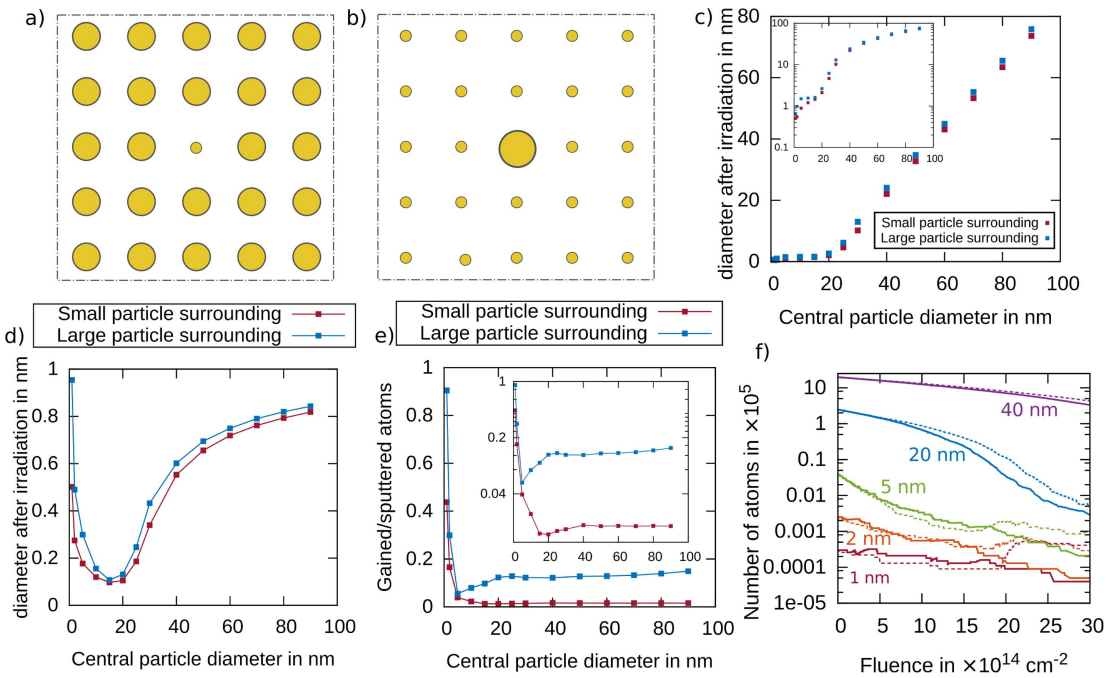

Figure 4. Schematic illustrations of the 5 × 5 squared patterns for the simulated situation for investigation of the dependence of the amount of redeposited atoms of the size of neighboring NPs for large (a) and small (b) neighbors. (c) Diameter of the central NP after the irradiation as a function of its initial size depending on the surrounding with 20 nm (red) and 50 nm (blue) sized NPs. (d) Ratio of the NP size after and before irradiation as a function of the initial size of central NPs. (e) Ratio of gained versus sputtered atoms for the central NP as a function of its initial diameter. The inset shows the plot with a logarithmic scale. (f) Evolution of the number of atoms in various central NPs as a function of ion fluence. The different colored curves show the different sizes of the central NP of 1 nm (red), 2 nm (orange), 5 nm (green), 20 nm (blue) and 40 nm (purple). The solid lines represent the neighboring NP of 20 nm, while the dashed lines represent the 50 nm NPs.

3.3. Influence of neighboring NP size on redeposition

We also performed simulations of two model systems with a central NP surrounded by two different groups of NPs, as it is shown in figures 4(a) and (b), in order to understand how the ratio of NP sizes affects the results. The groups of surrounding NPs were different by size, 20 or 50 nm in diameter and referred in the following simply as small and large neighboring NPs, respectively. The size did not vary within the group. Only the size of the central NP was varied from 1 to 100 nm. The results of these simulations are shown in figures 4(c)–(f).

As shown in figure 4(c), the size of the central particle after irradiation is changing similarly for both small and large neighboring NPs. This is in agreement with the results from figures 2(e) and (d). However, one consistent slight difference is obvious: the small surrounding NPs promote the faster erosion of the central NP.

The difference is better seen in figure 4(d), where the ratio of diameters after and before the irradiation is shown for both cases. The largest difference between the two simulated environments is seen for NP sizes smaller than 10 nm. While growing, the NP with the initially small size of 1 nm receives more atoms in the neighborhood of large NPs.

Figure 4(e) shows the ratio of collected to sputtered atoms as a function of the central NP diameter for both simulated cases. As expected, the ratio is larger for large surrounding NPs. The inset in figure 4(e) shows the plot with a logarithmic *y* axis. Clearly the ratio of gained versus sputtered atoms is about one order of magnitude larger for the case of large neighboring NPs compared to the small ones. Also, the slope of the linear regime is higher for the surroundings with larger particles. The evolution as a function of the ion fluence is shown in figure 4(f) for different centered NP sizes (different colors refer to different diameters). All NPs decrease in size with increasing ion fluence, except 1 nm sized NPs. These NPs remain in size, as visible in figures 4(d) and (e), or grow, as shown in figure 2. The evolution of the number of atoms in 1 and 2 nm NPs in the neighborhood of small and large NPs is clearly diverging between 1.5×10^{15} and 2×10^{15} cm^{-2}. The initial decreasing size trend of 2 nm NPs is changed to increasing one after 1.5×10^{15} cm^{-2} in the neighborhood of large NPs. This happens because the gain to sputter ratio is around ~0.9 for these NP sizes in these simulations. Both NPs, 1 and 2 nm, vanish after 2.1×10^{15} cm^{-2} if they are surrounded by small NPs. However, already at slightly larger NP sizes, e.g. for the 5 nm NP, the sputtering is a significantly stronger effect than the redeposition. For larger NPs, with 20 and 40 nm in diameter, the curves for the large surrounding NPs decrease in size slightly faster, but less pronounced than in the small NPs neighborhood. This leads to the conclusion that redeposition affects the evolution noticeably only for really small NPs with a diameter below 5 nm. Also, a surrounding of large NPs is

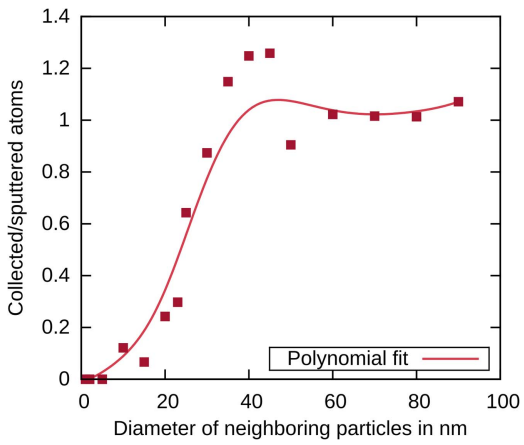

Figure 5. The ratio of collected versus sputtered atoms of a 1 nm sized NP in the center of the simulation volume as a function of the diameter of the neighboring NPs.

needed to provide the required material to compensate the sputtering loss. Since large NPs are more likely to be hit by ions, they emit more atoms for small NPs to collect them, compensating their own (marginal) sputtering. A small NP loses in total much less material (see figure 2(c)), which increases the chance for it to grow by redeposition.

Simulations with a 1 nm sized central NP were performed to investigate how big the neighboring NPs have to be in order to enable growth of the small NP. The simulation parameters were the same as in the previous simulations presented in this chapter. The diameters of the surrounding NPs were varied from 1 to 95 nm and irradiated with 3×10^{15} cm^{-2} Ga^{+} ions. The ratio of collected versus sputtered atoms as a function of the diameter of neighboring NPs for the 1 nm sized central NP is shown in figure 5. It is apparent that the surrounding NPs have to have at least a diameter of ~40 nm in order to provide enough material for central NP growth. For increasing neighboring NP diameters, the ratio of collected versus sputtered atoms saturates and does not increase further with increasing diameter. With a neighboring NPs diameter of 25 nm, the ratio of collected versus sputtered atoms is still ~0.6, which leads to a significant delay in shrinking. However, for neighbors smaller than ~20 nm in diameter we expect that sputtering is the dominating effect and even very small NPs shrink rapidly.

In conclusion, NPs with diameters between 1 and 2 nm are not expected to vanish in vicinity of large neighbors with diameters larger than ~20 nm or decrease in size delayed. They vanish if the neighboring NPs decreased enough in size so that the probability of redeposition becomes smaller than sputtering. Therefore, we expect that for high fluence irradiations all nanoparticles finally vanish rather than that a uniform distribution of small NPs establishes.

3.4. Comparison of experiment versus simulation

SEM images of the *in situ* experiments are shown in figures 6(a)–(c). During these experiments, NPs with the same initial size decreased with different rates. One can see three SEM images of different irradiation states of Au NPs on a Si substrate. Figure 6(a) shows the situation before irradiation with 30 keV Ga^{+} ions. Some NPs are marked and show the most interesting behavior during the irradiation. On the left hand side of the pictures, two NPs next to each other are marked with red circles (I and II). These NPs have approximately the same size. A third NP (III), near the center of the images, as the largest NP, is also marked. Over the process of irradiation, the NPs decrease in size due to sputtering. However, as shown in figure 6(b), NP II of the two initially equally sized NPs vanished after approximately 3×10^{15} cm^{-2}, while NP I still remains. The largest NP III decreased in size very little compared to the others. There are two possible mechanisms describing the observed behavior:

1. As described by Greaves *et al* [26], the sputtering yield depends on the angle between crystal lattice and ion beam direction. For small angles, the channeling effect leads to reduced sputtering due to less deposited energy when the ions are channeled. If the left of the two equally sized NPs has a lattice direction facing the ion beam, this would lead to a delayed size decrease. 2. Sputtered material could get redeposited on NPs lying next to a particle, which got hit by an ion. Since the two NPs have slightly different neighbors with different sizes, they might gain a different amount of material, which slows down the size decrease. This effect would be more pronounced for the large NP III, since it covers a large solid angle. One could expect a non-negligible amount of material redeposited on NP III, which leads to reduced shrinking of it.

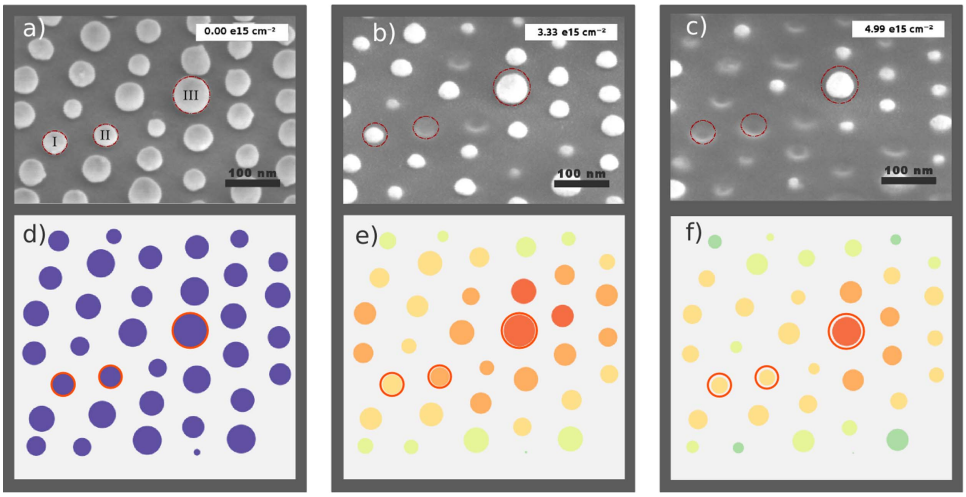

Figure 6. Comparison of SEM images of the *in situ* experiment (a)–(c) with the results obtained by the MC simulation (d)–(f). The left column shows the initial state, the middle column the situation after 3.3×10^{15} cm^{-2} and the right column after 5.0×10^{15} cm^{-2}. The simulation results were obtained by using the scaled Järvi model. The different colors of the particles in (e) and (f) represent the relative amount of redeposited to sputtered material from red (high) to green (low).

As shown in the simulations, the effect of redeposition compensates only about 12%–18% of the sputtered atoms, depending on the size and the surrounding. Thus, we performed a simulation where we used the SEM image of the initial NP array as an input arrangement to clarify whether channeling or redeposition is the key mechanism responsible for different sputtering rates. Figures 6(e) and (f) show the simulated NP evolution as a function of ion fluence in direct comparison to the experiment.

The simulation shows a smaller size decrease compared to the experiments. But more importantly, both NPs, I and II, decreased in both cases in almost the same way in the simulation. Also after 5.0×10^{15} cm^{-2}, NP I and II have almost the same size in the simulation. This leads to the conclusion that the sputtering of single NPs in experiments is depending on more parameters than the simulation takes into account. Thermally driven effects and cluster sputtering [26] can lead to higher sputtering yields for single ion impacts than taken into account by this MC simulation. Also NP–substrate-interaction is neglected in our present simulation.

Figure 7 shows a detailed investigation of the two initially almost equal sized NPs I and II using the MC simulation as a function of the ion fluence. The solid lines depict the simulations and the data points show the experimentally obtained results. In both cases, the NPs decrease in size almost with the same rate. Here, one can see also that none of the simulated particles vanish after the irradiation with 5×10^{15} cm^{-2}. The experimentally observed NPs decrease fast in size at the beginning, but remain almost constant in size for further 1×10^{15} cm^{-2} on the observed area. After 1×10^{15} cm^{-2}, both particles start shrinking with almost the same velocity as the simulation predicts. This results in very good agreement of simulation and experiment up to the fluence at which the particles vanish.

The simulation is well in line with the experiment. NP I and II could not be evaluated after ion fluences of 3.3×10^{15} cm^{-2} and 2.4×10^{15} cm^{-2}, respectively, due to increasing NP–substrate interactions. The NPs can not be distinguished from the substrate after the respective fluences as they start to sink into the substrate [37] and severe ion beam mixing starts. The experimentally obtained number of atoms does not reach 0 since the intermixing of Au of the NPs with the Si substrate in the experiment makes it hard to distinguish between the Au NP and the intermixing area on the substrate after a certain fluence [14, 31]. The NP–substrate-interaction leads to flattening of the NPs in the experiment, while the NPs barely decrease in size in the lateral direction.

Figure 7(b) shows the number of collected atoms as a function of the ion fluence for the simulation. The interesting fact here is that NP II, which is vanishing in the experiment, gains slightly more material than NP I. The reason for this might be the slightly larger diameter and thus the larger cross sectional area. The inset in figure 7(b) shows the ratio of gained versus sputtered atoms as a function of ion fluence. Over the whole simulated irradiation process, NP II compensates more sputtered material by redeposition. Nevertheless, both curves are practically parallel over the whole process. The difference between both curves is almost negligible for ion fluences larger than 1×10^{13} cm^{-2}. These results show, that redeposition cannot explain the different rates of shrinkage of NP I and II. Hence the channeling effect (see above) is most likely to explain the effect observed in the experiments.

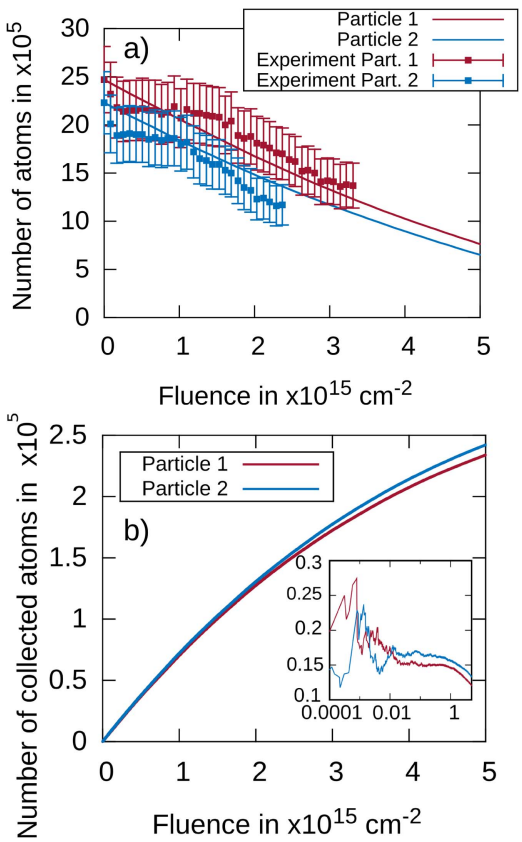

Figure 7. Simulation and experimental results for the two initially almost equal sized NPs from figure 6 as a function of ion fluence. The results for NP I is shown in red, NP II in blue color. The solid lines show the results for simulations using the scaled Järvi model. (a) Number of atoms as a function of the ion fluence. It is noticeable that both particles decrease in size almost with the same rate. The data points represent the experimental results. (b) Number of collected atoms as a function of the ion fluence. Particle II, which is decreasing faster in the experiment, gains slightly more atoms than particle I. The inset shows the fraction of gained versus sputtered atoms as a function of the number of impinged ions.

4. Conclusion

The irradiation of NP arrays with NPs of various sizes, which show a Gaussian size distribution, was simulated considering both sputtering and redeposition processes. The Gaussian size distribution was conserved. The difference between the mean diameters for simulations with and without redeposition was 2 nm after irradiation, whereas the situation without redeposition showed the smaller mean NP diameter after the irradiation. The mean NP diameter of both simulations matched the experimental values using a scaled Järvi's model. When the Järvi's original model was used, the simulation showed a smaller mean diameter of the NP sizes than observed in the experiments. On average, 12%–18% of the sputtered material was redeposited onto the particles according to the simulation for NP sizes larger than 30 nm. The behavior changes for smaller NP sizes. A minimum of the gained to sputtered atom ratio is observed around NP sizes where the sputtering yield reaches its maximum. For NPs smaller than 10 nm, the ratio increases again. NPs of 1 nm in diameter can even grow during ion irradiation due to redeposition from the neighboring particles.

The amount of redeposited material on NPs was investigated as a function of surrounding NP sizes. Redeposition is slightly stronger, if the NPs have large neighbors. Small NPs with sizes smaller than 10 nm obtain an increased amount of redeposited material compared to larger NP sizes for both small and large neighboring NPs, but only in the case of large neighbors; NPs with sizes of about 1 nm grow due to redeposition.

The process of redeposition is not the main factor in the experimentally observed effect when NPs having the equal sizes shrink with different rates. This effect might rather be attributed to channeling.

Acknowledgments

We thank the C Pacholski, S Scheeler and C Stanglmair for providing the Au nanoparticle samples and Dr Tommi Järvi for providing the software to implement his model. We also thank the BMBF for funding (BMBF

project PhoNa, contract no.03IS2101E & 03IS2101A) and the Max Planck Society. We also like to thank the reviewers of this manuscript for their competent comments.

References

[1] Novoselov K S, Geim A K, Morozov S V, Jiang D, Zhang Y, Dubonos S V, Grigorieva I V and Firsov A A 2004 Electric field effect in atomically thin carbon films *Science* **306** 666–9

[2] Iijima S and Ichihashi T 1993 Single-shell carbon nanotubes of 1-nm diameter *Nature* **363** 603–5

[3] Röder R, Ploss D, Kriesch A, Buschlinger R, Geburt S, Peschel U and Carsten R 2014 Polarization features of optically pumped CdS nanowire lasers *J. Phys. D: Appl. Phys.* **47** 394012

[4] Johannes A *et al* 2014 Enhanced sputtering and incorporation of Mn in implanted GaAs and ZnO nanowires *J. Phys. D: Appl. Phys.* **47** 394003

[5] Decoster S and Vantomme A 2009 Implantation-induced damage in Ge: strain and disorder profiles during defect accumulation and recovery *J. Phys. D: Appl. Phys.* **42** 165404

[6] Habenicht S, Bolse W, Feldermann H, Geyer U, Hofsäß H, Lieb K P and Roccaforte F 2000 Ripple topography of ion-beam—eroded graphite: a key to ion-beam—induced damage tracks *Europhys. Lett. EPL* **50** 209–15

[7] Pedrys R, Anders C and Urbassek H M 2015 Electronic sputtering of solid O_2 by keV Ne ions *Nucl. Instrum. Methods Phys. Res.* **354** 230–4

[8] Hamm R W and Hamm M E 2012 *Industrial Accelerators and their Applications* (Singapore: World Scientific)

[9] Schmidt B and Wetzig K 2013 *Ion Beams in Materials Processing and Analysis* (Vienna: Springer)

[10] Nastasi M, Mayer J W and Wang Y 2014 *Ion Beam Analysis: Fundamentals and Applications* (Boca Raton, FL: CRC Press)

[11] Hauffe W 1993 *Handbook of Ion Implantation Technology* (North-Holland: Elsevier) 1992. 700 S. 307 Abb. 28 Tab. ISBN 0-444-89735-6 *Cryst. Res. Technol.* **28** 978

[12] Bernas H 2010 *Materials Science with Ion Beams* vol 116 (Berlin: Springer)

[13] Ronning C, Borschel C, Geburt S and Niepelt R 2010 Ion beam doping of semiconductor nanowires *Mater. Sci. Eng.* R **70** 30–43

[14] Johannes A, Holland-Moritz H and Ronning C 2015 Ion beam irradiation of nanostructures: sputtering, dopant incorporation, and dynamic annealing *Semicond. Sci. Technol.* **30** 33001

[15] Ziegler J F, Ziegler M D and Biersack J P 2010 SRIM—the stopping and range of ions in matter (2010) *Nucl. Instrum. Methods Phys. Res.* B **268** 1818–23

[16] Sigmund P 1982 Kinetic theory of particle stopping in a medium with internal motion *Phys. Rev.* A **26** 2497–517

[17] Sigmund P 1987 Mechanisms and theory of physical sputtering by particle impact *Nucl. Instrum. Methods Phys. Res.* B **27** 1–20

[18] Järvi T T, Pakarinen J A, Kuronen A and Nordlund K 2008 Enhanced sputtering from nanoparticles and thin films: size effects *EPL Europhys. Lett.* **82** 26002

[19] Anders C, Bringa E M and Urbassek H M 2015 Sputtering of a metal nanofoam by Au ions *Nucl. Instrum. Methods Phys. Res.* B **342** 234–9

[20] Nietiadi M L, Sandoval L, Urbassek H M and Möller W 2014 Sputtering of Si nanospheres *Phys. Rev.* B **90** 45417

[21] Möller W and Eckstein W 1984 Tridyn—a TRIM simulation code including dynamic composition changes *Nucl. Instrum. Methods Phys. Res.* B **2** 814–8

[22] Schiettekatte F 2008 Fast Monte Carlo for ion beam analysis simulations *Nucl. Instrum. Methods Phys. Res.* B **266** 1880–5

[23] Borschel C and Ronning C 2011 Ion beam irradiation of nanostructures—a 3D Monte Carlo simulation code *Nucl. Instrum. Methods Phys. Res.* B **269** 2133–8

[24] Möller W 2014 TRI3DYN—collisional computer simulation of the dynamic evolution of 3-dimensional nanostructures under ion irradiation *Nucl. Instrum. Methods Phys. Res.* B **322** 23–33

[25] Sandoval L and Urbassek H M 2015 Collision-spike sputtering of Au nanoparticles *Nanoscale Res. Lett.* **10** 314–22

[26] Greaves G, Hinks J A, Busby P, Mellors N J, Ilinov A, Kuronen A, Nordlund K and Donnelly S E 2013 Enhanced sputtering yields from single-ion impacts on gold nanorods *Phys. Rev. Lett.* **111** 65504

[27] Diddens C and Linz S J 2013 Continuum modeling of particle redeposition during ion-beam erosion *Eur. Phys. J.* B **86** 397

[28] Diddens C and Linz S J 2013 Redeposition during ion-beam erosion can stabilize well-ordered nanostructures *EPL Europhys. Lett.* **104** 17010

[29] Smith R, Tagg M and Walls J 1984 *Vacuum Special Issue: Proc. 3rd Int. Conf. Low Energy Ion Beams (Loughborough University of Technology, UK)* ; deterministic models of ion erosion, reflection and redeposition *Vacuum* **34** 175–80

[30] Lindsey S and Hobler G 2012 The significance of redeposition and backscattering in nanostructure formation by focused ion beams *Nucl. Instrum. Methods Phys. Res.* B **282** 12–6

[31] Holland-Moritz H, Scheeler S, Stanglmair C, Pacholski C and Ronning C 2015 Enhanced sputter yields of ion irradiated Au nano particles: energy and size dependence *Nanotechnology* **26** 325301

[32] Sigmund P 1969 Theory of sputtering: I. Sputtering yield of amorphous and polycrystalline targets *Phys. Rev.* **184** 383–416

[33] Järvi T T and Nordlund K 2012 Sputtering of freestanding metal nanocrystals *Nucl. Instrum. Methods Phys. Res.* B **272** 66–9

[34] Samela J, Kotakoski J, Nordlund K and Keinonen J 2005 A quantitative and comparative study of sputtering yields in Au *Nucl. Instrum. Methods Phys. Res.* B **239** 331–46

[35] Ullrich S, Scheeler S P, Pacholski C, Spatz J P and Kudera S 2013 Formation of large 2D arrays of shape-controlled colloidal nanoparticles at variable interparticle distances *Part. Part. Syst. Charact.* **30** 102–8

[36] Schneider C A, Rasband W S and Eliceiri K W 2012 NIH Image to ImageJ: 25 years of image analysis *Nat. Methods* **9** 671–5

[37] Klimmer A, Ziemann P, Biskupek J, Kaiser U and Flesch M 2009 Size-dependent effect of ion bombardment on Au nanoparticles on top of various substrates: thermodynamically dominated capillary forces versus sputtering *Phys. Rev.* B **79** 155427